Cutting properties of deposited amorphous silicon in ultra-precision machining

Emil V. Jelenković[1], Suet To[1, *], Ling Chen[2], Gaobo Xiao[3], Zejia Zhao[1], Chak Yin Tang[2]

[1]State Key Laboratory of Ultra-Precision Machining Technology, Department of Industrial and Systems Engineering, The Hong Kong Polytechnic University, Hong Kong SAR, People's Republic of China

[2]Department of Industrial and Systems Engineering, The Hong Kong Polytechnic University, Hong Kong SAR, People's Republic of China

[3]School of Mechanical Engineering, Shanghai Jiao Tong University, Shanghai, People's Republic of China

*Corresponding author: Suet To
Email: Sandy.To@inet.polyu.edu.hk
Tel: +852 27666587
Fax: +852 27647657

Abstract

The widely used amorphous silicon material is often a deposited one. It is mainly applied in the electronic industry and shows to be a promising candidate for optical devices. The mechanical cutting of deposited amorphous silicon has not been reported so far, while ultra-precision machining of such material for optical devices can be superior to a lithographic approach. In this article, for the first time, cutting properties of deposited amorphous silicon are compared with those of single crystal silicon and polycrystalline silicon, using plunge cut experiment. It is found that the critical depth of cut and cutting forces for the amorphous silicon are close to those of single crystalline silicon in the easy-to-cut orientation. In comparison to the polycrystalline silicon, amorphous silicon has higher critical depth of cut and lower cutting force. This may allow machining of amorphous optical devices on different semiconductors and/or moulds on various materials with enhanced and isotropic critical depth of cut, reduced tool wear and simplified cutting control.

Keywords

Ultra-precision machining; Brittle-ductile cutting mode transition; Amorphous silicon; Micro machining

1. Introduction

Amorphous silicon (aSi) films are widely used in thin film transistors (TFTs) for large displays [1]. They are suitable for optical devices, such as optical sensing [2], x-ray imaging [3], both based on TFTs, and wave guides [4], etc. Their infrared properties are close to that of single crystal silicon [4, 5] and were exploited also for the fabrication of micro lenses by deposition and reflow of aSi on electron beam etched silicon substrate [5].

aSi films can be deposited by different techniques such as sputter deposition [6], low pressure chemical vapor deposition (LPCVD) [1], and plasma enhanced chemical vapor deposition (PECVD) [7], etc., in which hydrogen content can be controlled. They can

be grown at different rates and thicknesses on silicon and non-silicon substrates [8], suitable for different applications [1-5], and potentially mechanically machined into micro lenses and other structures which require the thickness of silicon films in the range of a few micrometers to few tens of micrometers. The mentioned deposition techniques are the standard and cheap processes applied in the semiconductor industry.

Machining of single crystal silicon (SCS) is difficult because of its hardness and brittleness. Consequently, the cutting tool wear is significant [9, 10], and silicon has to be cut within a critical depth of cut (CDC) to maintain ductile cutting [9-12]. Also, SCS is mechanically anisotropic. For instance, on silicon with (100) orientation, the CDC for the cutting direction of <100> is about two times larger than for cutting direction of <110> [10]. The dependence of CDC on cutting direction is reported widely [11, 12]. Therefore, when forming an optical surface on SCS, the cutting process, like the diamond turning, has to take into account anisotropic character of CDC [12].

Cutting amorphous silicon could be easier because its atoms have a low order arrangement. In such material, the elastic modulus, as well as hardness, are reduced [6, 13, 14], which may improve the tool life. Due to the random Si network, the mechanical anisotropy is lost, which may simplify the control of silicon cutting [12].

Although it was predicted that under certain condition the bulk aSi can be produced from liquid state in millimeter mm droplet sizes [15], it has not been realized practically. Even produced, it would be impractical for cutting because of its small size. On the other hand, it was shown that SCS, amorphized by 10 MeV implantation with fluorine ions, has reduced the tool wear and increased CDC [9]. The aforementioned result and possibility to fabricate micro lenses on amorphous silicon [5] encourages the investigation of cutting of amorphous silicon films for the purpose of fabrication of micron sized optical devices or molds for glass optical devices [16].

Small grain polycrystalline silicon (poly-Si), with random grain orientation, can offer isotropic cutting as well and can be attractive for the fabrication of optical devices. It has been reported that silicon lens array can be fabricated by ultra-precision machining of poly-Si [17]. To the best of our knowledge, the CDC and cutting forces of poly-Si have not been compared with deposited aSi.

In this article, aSi LPCVD films are deposited on SCS wafers and their cutting properties are characterized through a plunge cutting. The cutting of aSi is compared with the cutting of polycrystalline and single crystal silicon, where poly-Si films were obtained by microwave crystallization of aSi films. The cutting analysis is supported with x-ray diffraction (XRD), Raman spectroscopy and nanoindentation of the investigated silicon films.

2. Experiment

The amorphous films were deposited by LPCVD at 550 °C on silicon wafer to the thickness of 1.15 μm. The silicon substrates were single crystal wafer of (100) orientation, boron doped and with the resistivity of 5-25 Ohm-cm.

Microwave annealing of aSi was carried out in a microwave processing system (HAMiLab-HV3000, Synotherm, China) at a frequency of 2.45 GHz in vacuum of about 1x10-4 Pa. The specimens were placed inside a microwave kiln made with alumina. The annealing temperature was controlled by adjusting the microwave power and it was monitored via an infrared pyrometer (Raytek, USA). The annealing temperatures were 500, 600 and 700 °C, with the annealing time of 30 minutes for each temperature. After annealing, the specimens were cooled down gradually inside the chamber of the microwave system to ambient temperature. The aSi film annealed at

500 °C was expected to remain amorphous, and the annealing at 600 and 700 °C were expected to cause crystallization to polycrystalline films. These changes in crystallinity were checked with Raman spectrometer (Horiba Jobin-Yvon LabRam HR800) and x-ray diffraction (XRD) (Rigaku, SmartLab) with CuKα radiation operating at 45 kV and 200 mA. Theta/2theta mode was used and the scanning range of 2theta was 20-60°. The scanning speed was 2°/min.

The mechanical properties of a-Si and crystallized poly-Si film were evaluated with dynamic nanoindentation with a Berkovich tip to the maximum load of 50 mN using an iNano indenter. The size of the workpieces for the indentation tests was 1 × 1 cm. The reference used to monitor the nanoindentation system was a quartz stand, for which the hardness and modulus were known. The load frame stiffness and the tip area function were automatically calibrated according to the method proposed by Oliver et al. [18]. After the nanoindentation test, the hardness and modulus were extracted by the iNano software automatically.

The plunge cutting was performed on ultra-precision turning machine, Moore nanotech 350FG, on 1 cm x 1 cm samples, cut from experimental samples listed in Table 1, which were glued onto fixtures. The fixtures were mounted on the spindle of the machine using vacuum chuck. The single crystal diamond tool was fixed on a Kistler 95256C1 force transducer to measure the cutting force. The nose diameter, rake angle and the clearance were, respectively, 1.145 mm, -25° and 15° (tool #1), for cutting aSi and poly-Si. The mentioned tool parameters for cutting SCS were 1.495 mm, -25° and 10° (tool #2), respectively. For easier comparison with the cutting of SCS, some aSi samples were plunge cut with the later tool as well. For all grooves, the cutting speed was 2 mm/s. Each sample was cut 5-6 times. The control SCS wafer had the same specifications as wafers used as substrates for aSi deposition. Details of plunge cutting are summarized in Table 1.

Table 1. Description of samples and taper cutting parameters

<table>
<tr><th rowspan="2">Sample label</th><th rowspan="2">Silicon material</th><th rowspan="2">Silicon film thickness (μm)</th><th rowspan="2">Annealing temperature (°C)</th><th rowspan="2">Cutting direction</th><th colspan="3">Single crystal diamond tool parameters</th><th rowspan="2">Cutting speed (mm/s)</th></tr>
<tr><th>Nose radius (mm)</th><th>Rake angle (°)</th><th>Clearance angle (°)</th></tr>
<tr><td>A</td><td rowspan="2">SCS</td><td>-</td><td>-</td><td><110></td><td rowspan="3">1.495</td><td rowspan="7">-25</td><td rowspan="3">10</td><td rowspan="7">2</td></tr>
<tr><td>B</td><td>-</td><td>-</td><td><100></td></tr>
<tr><td>aSi</td><td rowspan="5">aSi film</td><td rowspan="5">1.15</td><td>-</td><td rowspan="5">N/A</td></tr>
<tr><td>W0</td><td>-</td><td rowspan="4">1.145</td><td rowspan="4">15</td></tr>
<tr><td>W3</td><td>500</td></tr>
<tr><td>W5</td><td rowspan="2">Poly-Si film (crystallized by annealing aSi film)</td><td>600</td></tr>
<tr><td>W4</td><td>700</td></tr>
</table>

3.Results and discussion

3.1 Structural characteristics of amorphous and crystallized films

Using XRD measurements (Fig.1) and Raman spectroscopy (Fig. 2), the deposited film was confirmed to be amorphous and remained amorphous after annealing at 500 ºC. The films were crystallized by annealing at 600 and 700 ° C (Fig. 1 and 2).

Three distinctive (111), (220) and (311) Bragg peaks are commonly observed in thermally [19] and microwave [1] annealed amorphous silicon with the preferred (111) orientation [1, 19] as in Fig. 1. The integrated intensities (in arbitrary units) of (111) peak after the annealing at 600 and 700 ºC were 438 and 610, respectively, indicating better crystallinity [20] for the film annealed at higher temperature. The sharp peak around 2θ of 33.9° is a forbidden (200) silicon reflection. It is caused by multiple diffractions from single crystal silicon and its intensity can vary from zero to high values, while its 2θ value can be in the range from 31 to 35° [21].

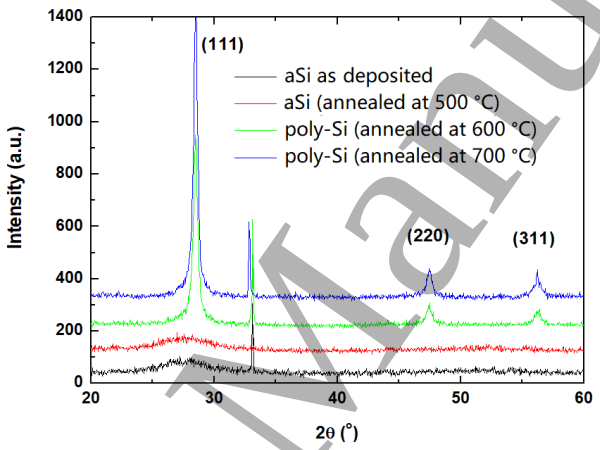

Fig.1 XRD of deposited films before and after annealing at different temperatures.

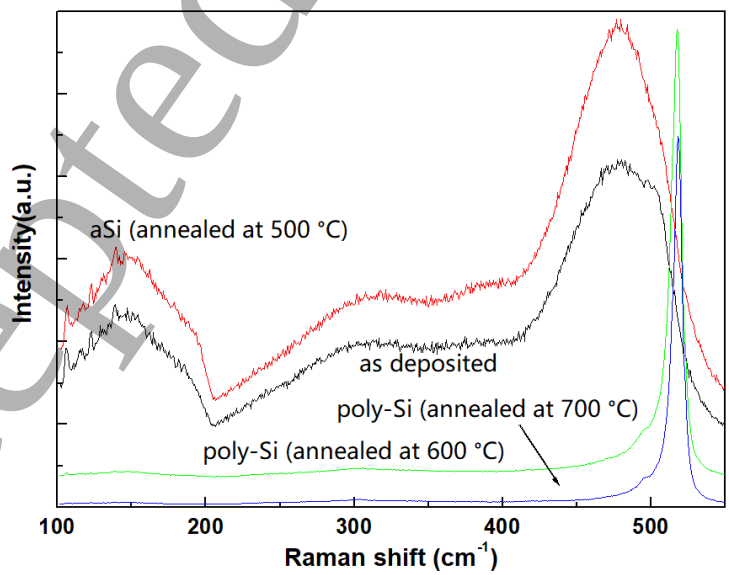

Figure 2. Raman spectra of deposited films before and after annealing.

The amorphous nature of a deposited film and one annealed at 500 ºC, are indicated by broad peaks at Raman shifts of about 146, 300, 400 and 479 cm^{-1} [22]. For the crystallized films, the Si–Si TO–LO phonon band is located at about 517 cm-1, a shift from 520 cm^{-1} value for single crystal silicon [23]. This reduced value indicates that the films are under tensile strain [23]. No hydrogen-related vibrations were detected in any silicon film in the range of 1800 to 2200 cm^{-1}, thus excluding its possible effect on mechanical properties and plunge cut in later analysis. This measurement is not shown. For the crystallized films, a tailing is observed in the lower values from the main peaks. Through fitting with the three peaks at 480 cm^{-1} (amorphous Si), 495 cm^{-1} (nano-crystal silicon) and at 517 cm^{-1} (crystalline silicon) [23], the percentage of crystallinity was calculated to be about 90% and 97 % for the films annealed at 600 and 700 ºC, respectively. The presence of amorphous phase in W5 and W4 films is also indicated by the weak broad peaks at around 146 cm^{-1}, with a more pronounced peak for W5.

3.2 Mechanical properties of films

Elastic modulus and hardness of different films are shown in Fig. 3. They were extracted from the depth of about 100 to 500 nm and were based on 10 measurements for each sample [24]. The hardness H and modulus E of the amorphous films were reduced in comparison to those of SCS in this investigation. The adopted values of SCS were 12.8 and 177.9 Pa, which are close to the previously published [24, 25]. The lower values for the amorphous silicon films are ascribed to the short-range arrangement of covalently bonded silicon atoms. The reduction in hardness and modulus for amorphous films from the values of SCS are about 10 % each. This hardness reduction is the same as for silicon amorphized by silicon ion implantation [26], while the modulus reduction in the same reference is 19 %. The XRD and Raman spectroscopy graphs indicate that the 700 ºC annealed films have higher crystallinity than those annealed at 600 ºC. After annealing, H and E values are about the same for both annealing temperatures and are 12.5 and 177.3, which are close to those measured for silicon with (100) orientation [24, 25].

The reduction of hardness and modulus was observed in aSi films sputter-deposited in argon plasma and the reduction can be manipulated with sputtering parameters, such as sputtering pressure, temperature and substrate bias [6]. Jiang et. al [13] reported that incorporation of a few percentages of hydrogen in the sputtered film can slash hardness of not-hydrogenated sputtered films by 40-60 %, which is a significantly greater reduction than in LPCVD films investigated in this article. On the other hand, PECVD films can be easily hydrogenated during the deposition process and it was shown that a few percentages of hydrogen can reduce the hardness [14]. It was also reported that small concentration of hydrogen in SCS, well below 1%, can modify the cutting behavior in an anisotropic way [10] and increase hardness and modulus [24]. Therefore, it will be compelling to explore the relation of mechanical properties of hydrogenated deposited aSi to the cutting properties in a future study.

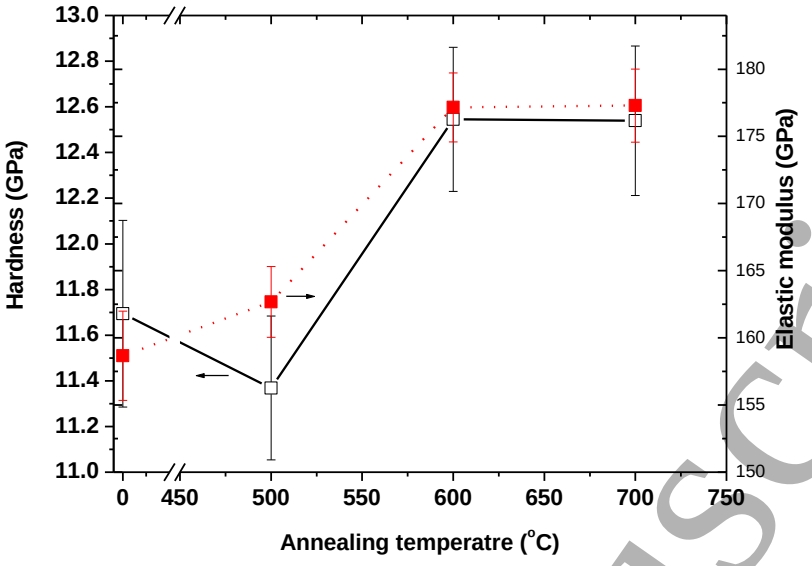

Fig. 3. Elastic modulus and hardness of as-deposited and annealed films.

3.3 Morphology and critical depth of cut

The grooves obtained by small angle plunge cut were examined by Nomarski microscope and Zygo optical profiler, Nexview NX2. Typical two-dimensional (2D) microscopic images of the grooves are shown in Fig. 4 for grooves cut out in SCS and silicon films. In the images, modes of cutting are described. The ductile cutting is characterized by a smooth and featureless surface. The random, brittle-cut, has small fractures and a rough surface or/and with the cleavage. The cleavage of silicon appears only for cutting SCS in <100> direction and appears after the ductile cutting. At a greater cutting depth, they are transformed into random fractures (Fig. 4a). It can be noticed that the grooves in aSi, poly-Si and for cutting SCS in <110> direction in SCS have initially a ductile regime of cutting, followed by a random-brittle appearance. In amorphous silicon and polycrystalline silicon there are not preferable cleavage planes, so only random fractures appear. Detailed discussion on the morphologies of the grooves in SCS from the orthogonal cutting point of view can be found in our prior work [10].

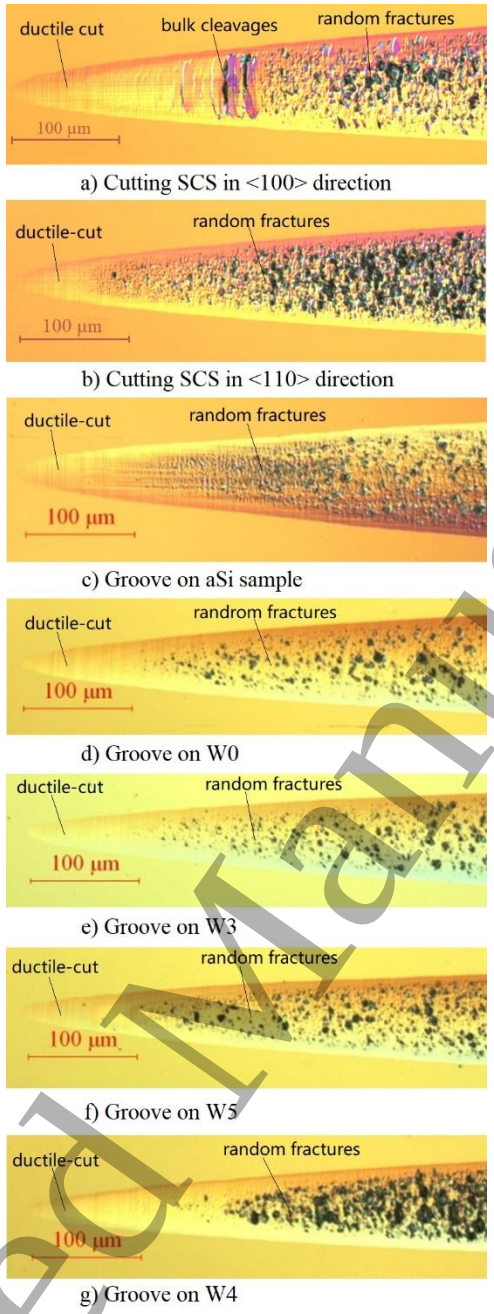

Fig. 4. Microphotographs of grooves on SCS (a., b.), aSi (c., d., e.) and poly-Si (f., g.).

The CDC is determined at the point where the random fracture starts using Zygo optical profiler [10]. The average CDCs with the standard deviation of the investigated samples are shown in Table 2. The CDC for SCS was in the range of ~ 100 -180 nm depending on the crystal orientations, and is consistent with the theoretical values of CDC reported by a number of studies [27-29] which predicted CDC in the range of ~ 60 – 220 nm. The CDC for aSi samples is close to the CDC for the cutting of SCS in <100> direction and it is larger by about 70 nm than the CDC for the cutting of SCS in <110> direction. This result should allow a greater flexibility of cutting and a more isotropic cutting process in the machining of amorphous silicon in comparison with the machining of single crystal silicon [12, 13]. The CDC of amorphous silicon (W0, W3) is larger than that of poly-Si. Overall, about CDC, cutting of amorphous silicon is

superior to the cutting poly-Si, and is more isotropic than that of single crystal silicon. But the difference in CDC for aSi material and poly-Si are smaller than the difference in the cutting of aSi and SCS in <110> direction.

Table 2 Average critical depth of cut

	SCS		aSi			Poly-Si	
Sample	A	B	aSi	W0	W3	W5	W4
CDC with tool #1 (nm)				215 ±28	204±25	169±15	189±7
CDC with tool #2 (nm)	99±29	180±14	171±17				

The results of CDCs in Table 2 should be addressed from the perspective of cutting parameters and the nature of aSi. As per the values in Table 2, the cutting with a smaller nose radius tool leads to a greater CDC. It was reported that CDC can be increased with a tool with more negative rake angle, while other cutting conditions being similar [11]. In the fly cutting test on (100) silicon and with 1.5 mm nose radius, -45^{o} rake angle and -10^{o} clearance, O'Connor et al. [30] reported qualitatively same results as in our case for A and B samples, though with smaller values for CDC which is possibly due to the much higher cutting speed they adopted. These examples indicate that CDC has a complex relation to the cutting parameters. Nevertheless, a comparative study of pairs SCS vs. aSi and aSi vs. poly-Si with the same tool for each pair shows that the CDC for deposited aSi is greater than the other two silicon materials.

One of the first cuttings of amorphous silicon was published by Fang et al. [9]. In their report, the amorphous silicon was produced by high energy fluorine implantation into SCS. The plunge cut of such silicon gave CDC of about 900 nm, which is about 4-5 time larger than for the deposited amorphous silicon in Table 2. In ion implanted single crystal silicon, the diamond lattice is destroyed, creating a disordered silicon arrangement, which is close to model of continuous random network [6]. Also, it was shown that the aSi films obtained by implantation of SCS with silicon ion have fractured toughness of 65 % higher than pristine SCS [26]. In contrast, the grown films are less consistent and dense due to the presence of boundaries among clusters consisting of short-range ordered silicon atoms [6]. Therefore, less uniform and less dense deposited film could be the reason for their smaller CDCs than the CDC of ion-implanted SCS.

3.4 Cutting force

The primary force (Fc) and thrust force (Ft) of the cut grooves were analyzed. The averaged cutting forces for cutting in <100> and <110> are compared to the cutting force of aSi film in Fig.5, while in Fig. 6, cutting forces for poly-Si and aSi films are

presented. It should be noted that for the two figures, two different tools were used (see Table 1). For clearer presentation and comparison, the values Ft are shown with negative values in Figs. 5 and 6.

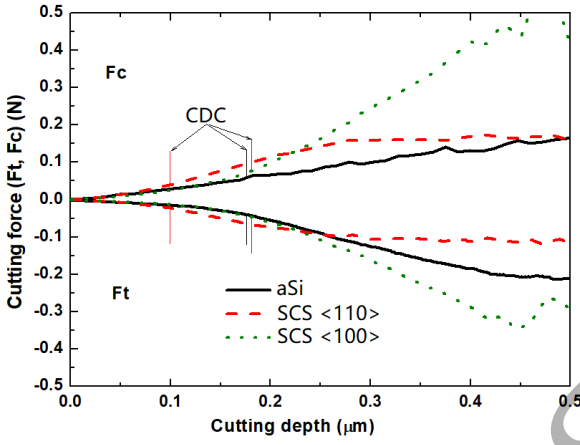

Fig.5. Comparison of cutting forces for SCS and aSi film.

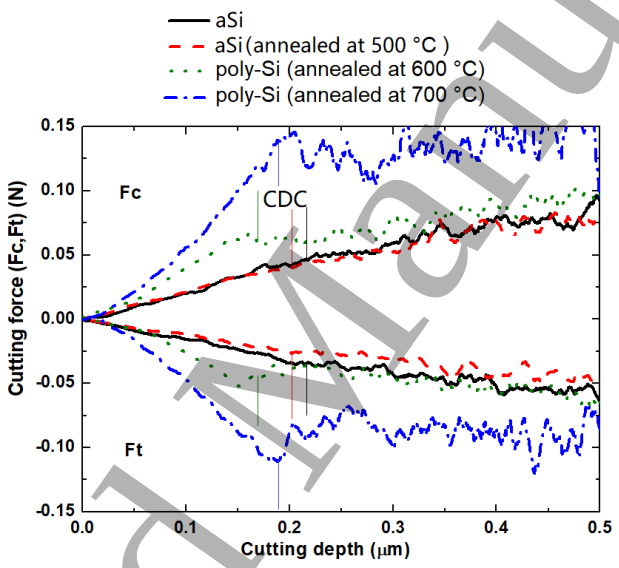

Fig.6. Comparison of cutting forces for aSi and poly-Si films.

Fc and Ft cutting forces in <100> cutting direction in the ductile regime are smaller than those in the <110> direction, which agrees with previous publications [10, 11]. What is important for this article, is that the cutting forces (Fc and Ft) for aSi are also smaller than the cutting force in <110> cutting direction, and very close to the cutting forces for cutting in <100> direction. Assuming that the CDC for the three samples (aSi, A and B) in Fig.4 is 180 nm (close to the CDC for aSi and B samples), the average cutting forces from 0-180 nm are calculated and listed in Table 3. These numerical values show that in general, the primary cutting force is larger than the thrust force for all three samples. This further means that the overall cutting force of amorphous Si, in comparison to cutting monocrystalline silicon, at CDC of about 180 nm will be smaller and in an isotropic way, simplifying the control of ultra-precision machining [12][30].

Table 3 Average cutting forces Fc and Ft for the depth ranges of 0-180 nm and 0-150 nm

Sample	Depth range (nm)	Average Fc (N)	Average Ft (N)
A	0-180	0.038	0.025
B	0-180	0.029	0.016
aSi	0-180	0.027	0.017
W0	0-150	0.015	0.012
W3	0-150	0.016	0.009
W5	0.150	0.029	0.019
W4	0.150	0.041	0.035

With the crystallization of aSi, the cutting forces (Fc and Ft) are increased. In this case, the Ft are smaller than the primary forces for all compared samples. While the cutting forces for the amorphous samples, i.e. W0 and W3, are about the same, the samples annealed at 700 ºC have obvious higher cutting forces than poly-Si film obtained at 600 ºC. This could be due to the slightly higher presence of amorphous phase in W5 sample despite similar hardness and elastic modulus. Such explanation could be related to the role of amorphous nano-size particles in the crystalline silicon on the cutting force. Namely, Wang et al. [31] observed in the surface region of silicon nano-size amorphous silicon defects after SCS was implanted with high energy oxygen ions. Through the frequency spectral analysis, it was observed that the implantation induced aSi and lower cutting force was observed in the ductile regime of cutting [31].

4. Conclusions

In this article, for the first time, mechanical cutting of LPCVD deposited amorphous silicon is reported. The cutting properties of aSi in the plunge cut experiment were compared to the cutting characteristics of single crystal silicon and polycrystalline silicon film from crystallization of amorphous silicon film. The main conclusions from this investigation are as follows.

(i) The critical depth of cut for amorphous silicon is close to that of single crystal silicon in <100> cutting direction and about 70 % higher than that in <110> cutting direction, allowing more isotropic machining processes.

(ii) The cutting forces in the ductile regime of cutting for the amorphous silicon are about the same as those when cutting single crystal silicon in <100> direction and reduced in comparison to those in <110> direction.

(iii) In comparison to polycrystalline silicon, amorphous silicon has larger critical depth of cut and lower cutting force.

This investigation is promising for the machining of nano/micro scale optical devices in amorphous silicon on semiconductors, or molds on silicon or some other materials.

Acknowledgement

The work described in this paper was partially supported by the Research Committee of The Hong Kong Polytechnic University (Projects G-YBEX and BBX5).

References

[1] Lu Y L, Lee Y J and Chao T S 2012 Simultaneous Activation and Crystallization by Low-Temperature Microwave Annealing for Improved Quality of Amorphous Silicon Thin-Film Transistors *Ecs Solid State Letters* **1** P1-P3

[2] Lin C L, Chen P S, Chang C H, Yu J S, Chang C and Tseng Y H 2017 A Hydrogenated Amorphous Silicon Thin-Film Transistor Optical Pixel Sensor for Ameliorating Influences of Ambient Light and Reflected Light *IEEE Journal of the Electron Devices Society* **5** 262-5

[3] Street R A, Wu X D, Weisfield R, Ready S, Apte R, Nguyen M and Nylen P 1996 Large area amorphous silicon x-ray imagers *Nuclear Instruments & Methods in Physics Research* **380** 450-4

[4] Shen L, Healy N, Mehta P, Day T D, Sparks J R, Badding J V and Peacock A C 2013 Nonlinear transmission properties of hydrogenated amorphous silicon core fibers towards the mid-infrared regime *Optics Express* **21** 13075-83

[5] Zuo H, Choi D Y, Gai X, Luther-Davies B and Zhang B 2017 CMOS compatible fabrication of micro, nano convex silicon lens arrays by conformal chemical vapor deposition *Optics Express* **25** 3069-76

[6] Kulikovsky V, Vorlíček V, Boháč P, Stranyánek M, Čtvrtlík R and Kurdyumov A 2008 Mechanical properties of amorphous and microcrystalline silicon films *Thin Solid Films* **516** 5368-75

[7] Iliescu C and Chen B 2007 Thick and low-stress PECVD amorphous silicon for MEMS applications *Journal of Micromechanics & Microengineering* **18** 252-6

[8] Cherenack K H, Hekmatshoar B, Sturm J C and Wagner S 2010 Self-Aligned Amorphous Silicon Thin-Film Transistors Fabricated on Clear Plastic at 300 °C *IEEE Transactions on Electron Devices* **57** 2381-9

[9] Fang F, Chen Y, Zhang X, Hu X and Zhang G 2011 Nanometric cutting of single crystal silicon surfaces modified by ion implantation *CIRP Annals-Manufacturing Technology* **60** 527-30

[10] G.B. X, S. T and E.V. J 2015 Effects of non-amorphizing hydrogen ion implantation on anisotropy in micro cutting of silicon *Journal of Materials Processing Technology* **under review**

[11] Yan J, Asami T, Harada H and Kuriyagawa T 2012 Crystallographic effect on subsurface damage formation in silicon microcutting *CIRP Annals-Manufacturing Technology* **61** 131-4

[12] Mao M and Yan J 2016 Ductile machining of single-crystal silicon for microlens arrays by ultraprecision diamond turning using a slow tool servo *International Journal of Machine Tools & Manufacture* **115**

[13] Jiang X, Reichelt K and Stritzker B 1989 The hardness and Young's modulus of amorphous hydrogenated carbon and silicon films measured with an ultralow load indenter *Journal of Applied Physics* **66** 5805-8

[14] Gope J, Kumar S, Parashar A and Dayal S 2015 Effect of Hydrogen Content and Bonding Environment on Mechanical Properties of Hydrogenated Silicon Films Deposited by High-Frequency PECVD Process *Isrn Nanomaterials* **2012**

[15] Shao Y, Spaepen F and Turnbull D 1998 An analysis of the formation of bulk amorphous silicon from the melt *Metallurgical & Materials Transactions A* **29** 1825-8

[16] He P, Li L, Yu J, Huang W, Yen Y C, Lee L J and Yi A Y 2013 Graphene-coated Si mold for precision glass optics molding *Optics Letters* **38** 2625-8

[17] Nitta T, Naruse M, Sekimoto Y, Mitsui K, Okada N, Karatsu K, Sekine M, Matsuo H, Noguchi T and Uzawa Y 2013 Beam Pattern Measurements of Millimeter-Wave Kinetic Inductance Detector Camera With Direct Machined Silicon Lens Array *IEEE Transactions on Terahertz Science & Technology* **3** 56-62

[18] Oliver W C and Pharr G M 2004 Measurement of hardness and elastic modulus by instrumented indentation: Advances in understanding and refinements to methodology *Journal of materials research* **19** 3-20

[19] Jelenkovic E V, Tong K Y and Ong C W 2002 Thin film transistors based on sputtered silicon and gate oxide films. In: *Electron Devices Meeting, 1996., IEEE Hong Kong,* pp 41-4

[20] Westra J M, Vavruňková V, Šutta P, Swaaij R A C M M v and Zeman M 2010 Formation of thin-film crystalline silicon on glass observed by in-situ XRD *Energy Procedia* **2** 235-41

[21] Zaumseil P 2015 High-resolution characterization of the forbidden Si 200 and Si 222 reflections *Journal of Applied Crystallography* **48** 528-32

[22] Volodin V A and Koshelev D I 2014 Quantitative analysis of hydrogen in amorphous silicon using Raman scattering spectroscopy *Journal of Raman Spectroscopy* **44** 1760-4

[23] Dimova-Malinovska D, Angelov O, Sendova-Vassileva M, Kamenova M and Pivin J C 2004 Polycrystalline silicon thin films on glass substrate *Thin Solid Films* **s 451–452** 303-7

[24] To S, Jelenković E V, Goncharova L V and Wong S F 2018 Mechanical characteristics of hydrogen-implanted crystalline silicon after post-implantation annealing *Vacuum* **152** 40-6

[25] Chang L and Zhang L 2009 Mechanical behaviour characterisation of silicon and effect of loading rate on pop-in: a nanoindentation study under ultra-low loads *Materials Science and Engineering: A* **506** 125-9

[26] Follstaedt D M, Knapp J A and Myers S M 2004 Mechanical properties of ion-implanted amorphous silicon *Journal of Materials Research* **19** 338-46

[27] Wang M, Wang W and Lu Z 2013 Critical cutting thickness in ultra-precision machining of single crystal silicon *The International Journal of Advanced Manufacturing Technology* **65** 843-51

[28] Venkatachalam S, Li X and Liang S Y 2009 Predictive modeling of transition undeformed chip thickness in ductile-regime micro-machining of single crystal brittle materials *Journal of materials processing technology* **209** 3306-19

[29] Arif M, Xinquan Z, Rahman M and Kumar S 2013 A predictive model of the critical undeformed chip thickness for ductile–brittle transition in nano-

machining of brittle materials *International Journal of Machine Tools and Manufacture* **64** 114-22

[30] O'Connor B P, Marsh E R and Couey J A 2005 On the effect of crystallographic orientation on ductile material removal in silicon *Precision Engineering* **29** 124-32

[31] Wang J, Chen R, Zhang X and Fang F 2017 Study on machinability of silicon irradiated by swift ions *Precision Engineering* **51**